Pattern selection in a predation model with self and cross diffusion*

Wang Wei-Ming(王玮明)[a)b)†], Wang Wen-Juan(王文娟)[b)],
Lin Ye-Zhi(林晔智)[c)], and Tan Yong-Ji(谭永基)[b)]

[a)] *College of Mathematics and Information Science, Wenzhou University, Wenzhou* 325035, *China*
[b)] *School of Mathematical Sciences, Fudan University, Shanghai* 200433, *China*
[c)] *Computer Sci-Tech Department, East China Normal University, Shanghai* 200062, *China*

(Received 29 July 2010; revised manuscript received 19 November 2010)

In this paper, we present the amplitude equations for the excited modes in a cross-diffusive predator–prey model with zero-flux boundary conditions. From these equations, the stability of patterns towards uniform and inhomogenous perturbations is determined. Furthermore, we present novel numerical evidence of six typical turing patterns, and find that the model dynamics exhibits complex pattern replications: for $\mu_1 < \mu \leq \mu_2$, the steady state is the only stable solution of the model; for $\mu_2 < \mu \leq \mu_4$, by increasing the control parameter μ, the sequence H_π-hexagons $\rightarrow$ H_π-hexagon-stripe mixtures $\rightarrow$ stripes $\rightarrow$ H_0-hexagon-stripe mixtures $\rightarrow$ H_0-hexagons is observed; for $\mu > \mu_4$, the stripe pattern emerges. This may enrich the pattern formation in the cross-diffusive predator–prey model.

Keywords: cross-diffusion, turing instability, pattern selection, amplitude equations
PACS: 47.54.–r, 87.23.Cc, 89.75.Kd **DOI:** 10.1088/1674-1056/20/3/034702

1. Introduction

Understanding of the spatial and temporal behaviours of interacting species in ecosystems is one of the central scientific problems in population ecology.[1−13] As one of several types of ecological interaction dynamics among multiple species in an ecosystem, predatory dynamics of interacting species have been investigated both in theory and in the field.[2,7,8,11,14−22]

The predator–prey system models the pursuit-evasion phenomenon—predators pursuing prey and prey escaping predators.[23] In such a system, there is a tendency that the prey stays away from the predators and the escape velocity of the preys may be taken to be proportional to the dispersive velocity of the predators. In the same manner, there is a tendency that the predators will get closer to the preys and the chase velocity of predators may be considered to be proportional to the dispersive velocity of the preys.[24] Therefore the problem of cross-diffusion arises, which was proposed first by Kerner[25] and first applied to competitive population systems by Shigesada *et al.*[26]

In recent years, there is the increasing interest in the stability behaviour of a predator–prey system in which the effects of self-diffusion and cross-diffusion[2,8,27−36] are considered. The cross-diffusion describes the population flux of one species due to the presence of other species. However, in the studies on spatiotemporal predator–prey system with functional response, little attention has been paid to the effect of cross-diffusion.

Most research on spatiotemporal predator–prey systems either focuses on the bifurcation phenomena with varying controlling parameter(s) or only gives the numerical results of some patterns. Little attention has been paid to the selection of the Turing patterns.

Thanks to the insightful work of many scientists over the decades, it is possible to study pattern selection by using the standard multiple-scale analysis. The key to this method is the so-called amplitude equations.[10,37−49] The amplitude equations have been discussed in some reaction–diffusion systems, such as Brusselator model,[37−39,47] Lengyel–Epstein model,[40] and so on.

In the present paper, we focus mainly on the dynamics of pattern selection in the predator–prey model. The rest of this paper is organized as follows. In Section 2, we introduce the model and give a general survey of the linear stability analysis and bifurcations with zero-flux boundary conditions. In Sec-

*Project supported by the Natural Science Foundation of Zhejiang Province, China (Grant No. Y7080041), and the Shanghai Postdoctoral Scientific Program, China (Grant No. 09R21410700).
†Corresponding author. E-mail: weimingwang2003@163.com
© 2011 Chinese Physical Society and IOP Publishing Ltd

tion 3, we use the multiple-scale method to derive the amplitude equations and discuss the results of Turing pattern formation via numerical simulations. Finally, conclusions and remarks are presented in Section 4.

2. Model and linear stability analysis

With the Michaelis–Menten or Holling II-type ratio-dependence functional response and logistic prey growth, the predator–prey model under consideration takes the form of

$$\begin{aligned}\frac{\mathrm{d}N}{\mathrm{d}t} &= rN(1-\frac{N}{K})-\frac{cNP}{N+mP},\\ \frac{\mathrm{d}P}{\mathrm{d}t} &= P\left(\frac{fN}{N+mP}-d\right),\end{aligned} \tag{1}$$

where $N(t)$ and $P(t)$ represent the population densities of prey and predator, respectively; r, K, m and d are the positive constants for prey intrinsic growth rate, carrying capacity, half saturation constant and the death rate of the predators P, respectively; c is the maximum prey death rate due to predation for an infinite number of predators; f is the maximum (asymptotic) predator growth rate for an infinite number of prey.

For simplicity, we nondimensionalize model (1) with the following scaling:[50]

$$N \to KN, \quad P \to KP/m, \quad t \to mt/c.$$

Then model (1) converts into

$$\begin{aligned}\frac{\mathrm{d}N}{\mathrm{d}t} &= \alpha N(1-N)-\frac{NP}{N+P},\\ \frac{\mathrm{d}P}{\mathrm{d}t} &= -\beta P+\frac{\gamma NP}{N+P},\end{aligned} \tag{2}$$

where

$$\alpha=\frac{rm}{c}, \quad \beta=\frac{dm}{c}, \quad \gamma=\frac{fm}{c}.$$

As shown in Refs. [50]–[52], by a change of the independent variable $t \to (N+P)t$, model (2) in the first quadrant is equivalent to the polynomial system

$$\begin{aligned}\frac{\mathrm{d}N}{\mathrm{d}t} &= \alpha N(1-N)(N+P)-NP,\\ \frac{\mathrm{d}P}{\mathrm{d}t} &= -\beta P(N+P)+\gamma NP.\end{aligned} \tag{3}$$

The corresponding spatial model to expression (3) with self-diffusion and cross-diffusion is as follows:

$$\begin{aligned}\frac{\partial N}{\partial t} &= \alpha N(1-N)(N+P)-NP\\ &\quad +d_{11}\nabla^2 N+d_{12}\nabla^2 P,\\ \frac{\partial P}{\partial t} &= -\beta P(N+P)+\gamma NP\\ &\quad +d_{21}\nabla^2 N+d_{22}\nabla^2 P,\end{aligned} \tag{4}$$

where the nonnegative constants, d_1 and d_2, are the diffusion coefficients of prey and predator, respectively; d_{12} and d_{21}, called cross-diffusion coefficients, describe the respective population fluxes of preys and predators resulting from the presence of the other species, respectively. Model (4) is to be analysed under the following non-zero initial conditions:

$$\begin{aligned}&N(x,y,0)>0, \quad P(x,y,0)>0,\\ &(x,y)\in\Omega=[0,Lx]\times[0,Ly],\end{aligned} \tag{5}$$

and zero-flux boundary conditions

$$\frac{\partial N}{\partial n}=\frac{\partial P}{\partial n}=0, \quad (x,y)\in\partial\Omega. \tag{6}$$

In the above, Lx and Ly denote the sizes of the system in the directions of x and y, respectively; n is the outward unit normal vector of the boundary $\partial\Omega$ which is assumed to be smooth. The main reason for choosing such boundary conditions is that we are interested in the self-organization of the pattern—zero-flux conditions imply no external input.

Model (3) has a uniform stationary state $(N,P)=(1,0)$ independent of the control parameters α, β, γ, and it corresponds to the prey being at its carrying capacity with no predators. Another equilibrium point depends on the parameters α, β and γ, and is given implicitly by

$$N^*=\frac{\alpha\gamma+\beta-\gamma}{\alpha\gamma}, \quad P^*=\frac{\gamma-\beta}{\beta}N^*. \tag{7}$$

In the presence of diffusion, set $N=N^*+\tilde{N}$ and $P=P^*+\tilde{P}$, where $|\tilde{N}|, |\tilde{P}| \ll 1$, the stationary state can become unstable to a nonuniform perturbation

$$\begin{aligned}&\tilde{N}(\boldsymbol{r},t)\sim\exp(\lambda t+\mathrm{i}\,\boldsymbol{k}\cdot\boldsymbol{r}),\\ &\tilde{P}(\boldsymbol{r},t)\sim\exp(\lambda t+\mathrm{i}\,\boldsymbol{k}\cdot\boldsymbol{r}), \quad \boldsymbol{r}=(x,y),\end{aligned}$$

where $\boldsymbol{k}\cdot\boldsymbol{k}=k^2$, k and λ are the wave-number and frequency, respectively. And the Turing instability occurs when the real part of an eigenvalue of the linear operator

$$\mathcal{L} = \begin{bmatrix} -\dfrac{(\alpha\gamma+\beta-\gamma)\left(\alpha\gamma^2-\gamma^2+\beta^2\right)}{\alpha\beta\gamma^2} - d_{11}k^2 & -\dfrac{(\alpha\gamma+\beta-\gamma)\beta}{\alpha\gamma^2} - d_{12}k^2 \\ \dfrac{(\alpha\gamma+\beta-\gamma)(-\beta+\gamma)^2}{\alpha\beta\gamma} - d_{21}k^2 & -\dfrac{(\alpha\gamma+\beta-\gamma)(-\beta+\gamma)}{\alpha\gamma} - d_{22}k^2 \end{bmatrix}$$

becomes positive, that is, when the determinant $\det(\mathcal{L}) < 0$ and trace $(\mathcal{L}) < 0$. And the critical value of the Turing bifurcation is defined by the following equation:

$$\alpha_{\rm c} = -\frac{1}{d_{22}^2\gamma^2}[\beta^2\Big((d_{11}d_{22}-2d_{12}d_{21}+d_{12}d_{22})\gamma - d_{22}(d_{21}-d_{22})\Big) - \beta\gamma^2(d_{11}d_{22}-2d_{12}d_{21} + 2d_{12}d_{22}) + \gamma^2 d_{22}(\gamma d_{12}-d_{22}) + 2\Upsilon], \tag{8}$$

where

$$\Upsilon = \sqrt{\beta\gamma(\beta-\gamma)(d_{21}\beta-d_{22}\beta+d_{22}\gamma)(d_{12}\gamma^2-d_{12}\beta\gamma-d_{22}\beta)(d_{11}d_{22}-d_{12}d_{21})}. \tag{9}$$

And the critical wavenumber $k_{\rm c}$ is given by

$$k_{\rm c}^2 = \sqrt{\frac{(\alpha\gamma+\beta-\gamma)^3(-\beta+\gamma)}{\alpha^2\beta\gamma^2(d_{11}d_{22}-d_{12}d_{21})}}. \tag{10}$$

The linear stability analysis yields the phase diagram with the parameter set

$$\{\beta,\gamma,d_{11},d_{12},d_{21},d_{22}\} = \{0.25,\ 0.50,\ 0.0125,\ 0.005,\ -0.001,\ 1.0\} \tag{11}$$

as shown in Fig. 1. The Turing bifurcation line separates the parametric space into two domains.

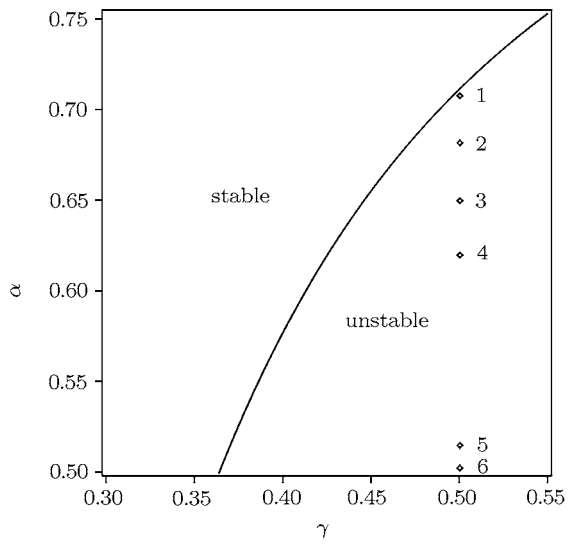


Fig. 1. Phase diagram for model (4) with parameter set (11). Turing bifurcation curve separates the parametric space into two domains. The domain above the curve is stable for all pairs of (γ,α); while the domain below the curve is unstable for (γ,α), and Turing patterns emerge. The coordinates (γ,α) of points '1' (0.5, 0.708), '2'(0.5, 0.682), '3'(0.5, 0.65), '4'(0.5, 0.62), '5'(0.5, 0.515), '6'(0.5, 0.5025) are corresponding to those in Fig.4, respectively.

The domain above the curve is stable for all pairs of (γ,α), that is, there is no diffusive instability. While the domain below the curve, called the 'Turing space', is unstable for (γ,α), and diffusive instability emerges, i.e., Turing patterns emerge.

We plot in Fig. 2 the dispersion relations corresponding to several values of bifurcation parameter α while keeping the others fixed with the set (11). In Fig. 2, curve b corresponds to the critical Turing value $\alpha^* = 0.7112215740$. When $\alpha = 0.71 < \alpha^*$ (e.g., curve a in Fig. 2), the Turing instability occurs, while $\alpha = 0.715 > \alpha^*$ (e.g., curve c in Fig. 2), the Turing instability decays. That is to say, when $\alpha > \alpha^*$, the steady state is the only stable solution of model (4).

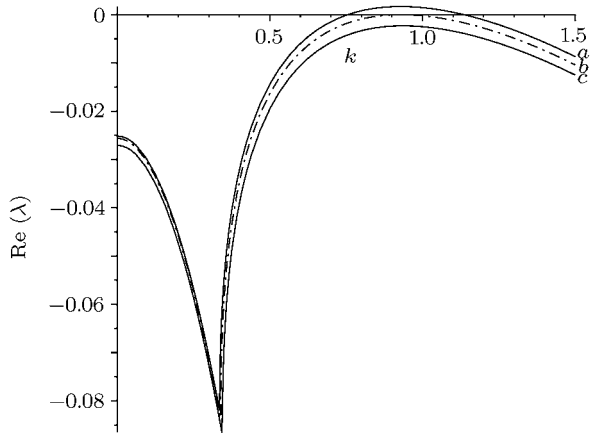


Fig. 2. Variations of dispersion relations of model (4) with the parameter set (11). When $\alpha = 0.71$, the Turing instability occurs (curve a); when $\alpha = 0.7112215740$ (the critical Turing bifurcation value), the Turing instability is in a critical state (curve b); when $\alpha = 0.715$, the Turing instability decays (curve c).

From the above analysis, we can obtain the conditions of Turing instability for model (4) and determine

the conditions of the emergency of Turing pattern. But we cannot determine the selection and competition of Turing patterns. In the next section, we shall consider the selection of Turing patterns close to the onset $\alpha = \alpha_c$.

3. Pattern selection

3.1. Amplitude equations

In the case close to onset $\alpha = \alpha_c$, the eigenvalues associated with the critical modes are close to zero, so that they are slowly varying modes, whereas the off-critical modes relax quickly, and only perturbations with k around k_c need to be considered. The whole dynamics can therefore be reduced to the dynamics of the active slow modes, which makes the fast stable modes slave.[37] The stabilities and the selections of the different patterns close to the onset can be derived from the amplitude equations that govern the dynamics behaviours of these active modes. Turing patterns (e.g., hexagonal and stripe patterns) are thus well described by a system of three active resonant pairs of modes $(\boldsymbol{k}_i, -\boldsymbol{k}_i)$ $(i = 1, 2, 3)$, two of which makes an angle of $2\pi/3$ and $|\boldsymbol{k}_i| = k_c$.

In the case close to onset $\alpha = \alpha_c$, the solutions of model (4) can be expanded into

$$\begin{aligned}\boldsymbol{U} = \boldsymbol{u}_0 \cdot \sum_{j=1}^{3} [A_j \exp(\mathrm{i}\,\boldsymbol{k}_j \cdot \boldsymbol{r}) \\ + \overline{A}_j \exp(-\mathrm{i}\,\boldsymbol{k}_j \cdot \boldsymbol{r})],\end{aligned} \tag{12}$$

where

$$\boldsymbol{u}_0 = \left(\frac{1}{d_{22}\gamma(d_{22}(\gamma^2 - 2\beta\gamma + \beta^2) + d_{21}\beta(\gamma - \beta))} (d_{12}\gamma(\gamma - \beta)(d_{22}\gamma + d_{21}\beta - d_{22}\beta) + \Upsilon), 1 \right)^{\mathrm{T}}$$

(Υ is defined as Eq. (9)) determines the direction of the eigenmodes in concentration space (i.e., the ratio N/P), A_j and conjugate $\overline{A}_j$ are, respectively, the amplitudes associated with modes $\boldsymbol{k}_j$ and $-\boldsymbol{k}_j$. From standard multiple-scale analysis, up to third order in the perturbations, the spatiotemporal evolution of the amplitud A_j is described by the amplitude equations:

$$\begin{cases} \tau_0 \dfrac{\partial A_1}{\partial t} = \mu A_1 + h\,\overline{A}_2\overline{A}_3 - \Big[g_1|A_1|^2 + g_2(|A_2|^2 + |A_3|^2)\Big]A_1, \\ \tau_0 \dfrac{\partial A_2}{\partial t} = \mu A_2 + h\,\overline{A}_1\overline{A}_3 - \Big[g_1|A_2|^2 + g_2(|A_1|^2 + |A_3|^2)\Big]A_2, \\ \tau_0 \dfrac{\partial A_3}{\partial t} = \mu A_3 + h\,\overline{A}_1\overline{A}_2 - \Big[g_1|A_3|^2 + g_2(|A_1|^2 + |A_2|^2)\Big]A_3, \end{cases} \tag{13}$$

where $\mu = (\alpha_c - \alpha)/\alpha$ is a normalized distance to onset. Notably, for model (4), the stationary state becomes Turing unstable when the bifurcation parameter α decreases, so the distance to onset, μ, increases when the bifurcation parameter α decreases.

The form of Eq. (13) is general for Turing bifurcations, the exact expressions of the coefficients are specified to the model. For more details about calculating coefficients τ_0, h, g_1 and g_2, readers may refer to Refs. [41], [46] and [53]. But the expressions of these coefficients are too complicated to be included here. For simplicity, we omit the exact expressions of these coefficients and only give a numerical example. If readers are interested in these computations, please contact the authors.

With fixed parameter set (11), the coefficients τ_0, h, g_1, and g_2 of Eq. (13) are

$$h = 0.9168602988, \quad g_1 = 9.432584229, \quad g_2 = 20.05800024. \tag{14}$$

3.2. Amplitude instability

Let $A_j = \rho_j \exp\varphi_j$ $(j = 1, 2, 3)$, amplitude equations in Eq.(13) can be written as follows:

$$\begin{aligned} \tau_0 \frac{\partial \varphi}{\partial t} &= -h \frac{\rho_1^2\rho_2^2 + \rho_1^2\rho_3^2 + \rho_2^2\rho_3^2}{\rho_1\rho_2\rho_3} \sin\varphi, \\ \tau_0 \frac{\partial \rho_1}{\partial t} &= \mu\rho_1 + h\rho_2\rho_3\cos\varphi \\ &\quad - g_1\rho_1^3 - g_2(\rho_2^2 + \rho_3^2)\rho_1, \\ \tau_0 \frac{\partial \rho_2}{\partial t} &= \mu\rho_2 + h\rho_1\rho_3\cos\varphi \\ &\quad - g_1\rho_2^3 - g_2(\rho_1^2 + \rho_3^2)\rho_2, \\ \tau_0 \frac{\partial \rho_3}{\partial t} &= \mu\rho_3 + h\rho_1\rho_2\cos\varphi \\ &\quad - g_1\rho_3^3 - g_2(\rho_1^2 + \rho_2^2)\rho_3, \end{aligned} \tag{15}$$

where $\varphi = \varphi_1 + \varphi_2 + \varphi_3$.

Dynamical system (15) possesses four kinds of solutions as follows.[45,54]

(i) The conductive state (O), given by

$$\rho_1 = \rho_2 = \rho_3 = 0, \tag{16}$$

is stable for

$$\mu < \mu_2 = 0, \tag{17}$$

and unstable for $\mu > \mu_2$.

(ii) Stripes, given by

$$\rho_1 = \sqrt{\frac{\mu}{g_1}} \neq 0, \quad \rho_2 = \rho_3 = 0, \tag{18}$$

are stable for

$$\mu < \mu_3 = \frac{h^2 g_1}{(g_2 - g_1)^2}, \tag{19}$$

and unstable for $\mu > \mu_3$.

(iii) Hexagons (H_0, H_π), given by

$$\rho_1 = \rho_2 = \rho_3 = \frac{|h| \pm \sqrt{h^2 + 4(g_1 + 2g_2)\mu}}{2(g_1 + 2g_2)} \tag{20}$$

with $\varphi = 0$ or π, exist for

$$\mu > \mu_1 = \frac{-h^2}{4(g_1 + 2g_2)}. \tag{21}$$

The solution $\rho^+ = \dfrac{|h| + \sqrt{h^2 + 4(g_1 + 2g_2)\mu}}{2(g_1 + 2g_2)}$ is stable only for

$$\mu < \mu_4 = \frac{2g_1 + g_2}{(g_2 - g_1)^2} h^2, \tag{22}$$

and $\rho^- = \dfrac{|h| - \sqrt{h^2 + 4(g_1 + 2g_2)\mu}}{2(g_1 + 2g_2)}$ is always unstable.

(iv) The 'mixed states', given by

$$\rho_1 = \frac{|h|}{g_2 - g_1}, \quad \rho_2 = \rho_3 = \sqrt{\frac{\mu - g_1 \rho_1^2}{g_1 + g_2}} \tag{23}$$

with $g_2 > g_1$, exist for $\mu > \mu_3$ and are always unstable.

With fixed parameter set (11), one can obtain

$$\begin{aligned} &\mu_1 = -0.004241457212, \\ &\mu_2 = 0, \quad \mu_3 = 0.07023363427, \\ &\mu_4 = 0.2898161871. \end{aligned} \tag{24}$$

The existence limit and the stability limit of the solutions, each as a function of the scaled bifurcation parameter μ, are ordered according to the scheme in Fig. 3. Stable branches H_0 and H_π are mutually exclusive. With the parameter set (11), the stable branch is H_0 because $h = 0.9168602996 > 0$. A subcritical hexagonal branch comes out first at $\mu = \mu_1 = -0.004241457212 < 0$ but it is destablized stability when $\mu > \mu_4 = 0.2898161871$. The supercritical stripe state branch is unstable close to the critical point but becomes stable for $\mu > \mu_3 = 0.07023363427$. In the range $\mu_3 < \mu < \mu_4$ both branches (i.e., H_0 and stripe 'S') are stable.

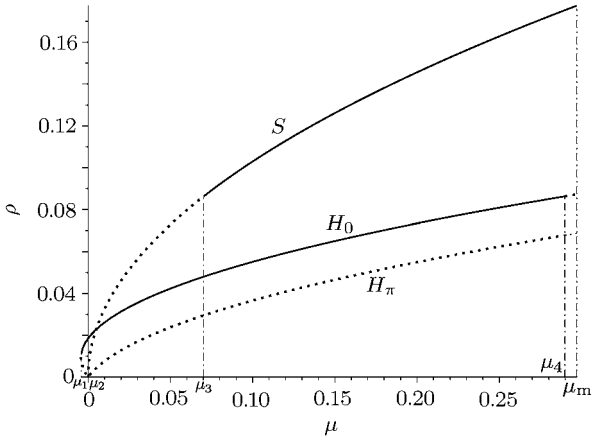


Fig. 3. Bifurcation diagram for model (4) with parameter set (11). H_0: hexagonal pattern with $\varphi = 0$; H_π: hexagonal pattern with $\varphi = \pi$; S: stripe pattern. —: stable state, - - -: unstable state. And, $\mu_1 = -0.004241457212$ (corresponding to $\alpha = 0.7142510392$), $\mu_2 = 0$ ($\alpha = 0.7112215740$), $\mu_3 = 0.07023363427$ ($\alpha = 0.6612698981$), $\mu_4 = 0.2898161871$ ($\alpha = 0.5050980492$). And the minimum $\alpha = 0.5$ corresponds to maximum $\mu_m = 0.2969842053$.

3.3. Pattern formation

In this subsection, we present qualitative results from our extensive numerical simulations of the spatially extended model (4) in two-dimensional (2D) spaces. In all our numerical simulations employed are the zero-flux boundary conditions (i.e., Eqs. (5) and (6)) with a system size of $Lx \times Ly$, where $Lx = Ly = 100$ discretized through $x \to (x_0, x_1, x_2, \ldots, x_n)$ and $y \to (y_0, y_1, y_2, \ldots, y_n)$, with $n = 300$. Other parameters are fixed as $\beta = 0.25, \gamma = 0.50, d_{11} = 0.0125$, $d_{12} = -0.005$, $d_{21} = 0.001$ and $d_{22} = 1.0$ in time steps of 0.025. We use the standard five-point approximation for the two-dimensional Laplacian with the zero-flux boundary conditions.

Presented in Fig. 4 are the numerical simulations, showing typical stationary pictures for the distribution of prey N of model (4) arising from random initial conditions for several values of μ.

(i) **Pattern selection when** $\mu_2 < \mu < \mu_3$: there are two categories of Turing patterns.

Figure 4(a) shows H_π-hexagons, where $\mu = 0.0045296348 > \mu_2$, i.e., $\alpha = 0.71$ and when $t = 10000$, there is a Turing pattern consisting of black (minimum density of N) hexagons on a white (maximum density of N) background, i.e., isolated zones with low population densities. It is noteworthy that $\mu = 0.0045296348$, i.e., $\alpha = 0.708$, refers to the point '1' in Fig. 1.

Figure 4(b) displays H_π-hexagon-stripe mixtures: $\mu = 0.0410864561 < \mu_3$, i.e., $\alpha = 0.682$ (the point '2' in Fig. 1). Some stripes emerge, and the remainder of the holes pattern remains time independent.

(ii) **Pattern selection when** $\mu_3 < \mu < \mu_4$: there are three categories of Turing patterns.

Figure 4(c) shows stripes, where $\mu = 0.0860794670 > \mu_3$, i.e., $\alpha = 0.65$ (the point '3' in Fig. 1), and model dynamics exhibits a transition from stripe-hole growth to stripes replication, i.e., holes decay and the stripes pattern emerges.

Figure 4(d) displays H_0-hexagon-stripe mixtures, where $\mu = 0.1282604146 > \mu_3$, i.e., $\alpha = 0.62$ (the point '4' in Fig. 1), and stripes and spots coexist in the spatial domain.

Figure 4(e) exhibits H_0-hexagons, where $\mu = 0.2758937315$, i.e., $\alpha = 0.515$ (the point '5' in Fig. 1), and the random perturbation leads to the formation of spots, which is time-independent.

(iii) **Pattern selection when** $\mu > \mu_4$: there is one kind of Turing pattern–stripes pattern.

Figure 4(f) as an example, indicates the stripe pattern with $\mu = 0.2934691263$, i.e., $\alpha = 0.505$ (the point '6' in Fig. 1), which is time-dependent.

From Fig. 4, one can see that the values of concentration N are represented in a gray scale varying from black (minimum) to white (maximum). For $\mu_2 < \mu < \mu_4$ (i.e., $0 < \mu < 0.2898161886$), as control parameter μ increases, the sequence H_π hexagons $\rightarrow$ H_π-hexagon-stripe mixtures $\rightarrow$ stripes $\rightarrow$ H_0-hexagon-stripe mixtures $\rightarrow$ H_0-hexagons is observed. When $\mu > \mu_4$, the stripe pattern emerges. Notably, in these cases, the distance to onset (i.e., μ) decreases when α increases. That is to say, for $0.5050980481 < \alpha < 0.7112215740$, as bifurcation parameter α increases, the sequence H_0-hexagons $\rightarrow$ H_0-hexagon-stripe mixtures $\rightarrow$ stripes $\rightarrow$ H_π-hexagon-stripe mixtures $\rightarrow$ H_π-hexagons is observed.

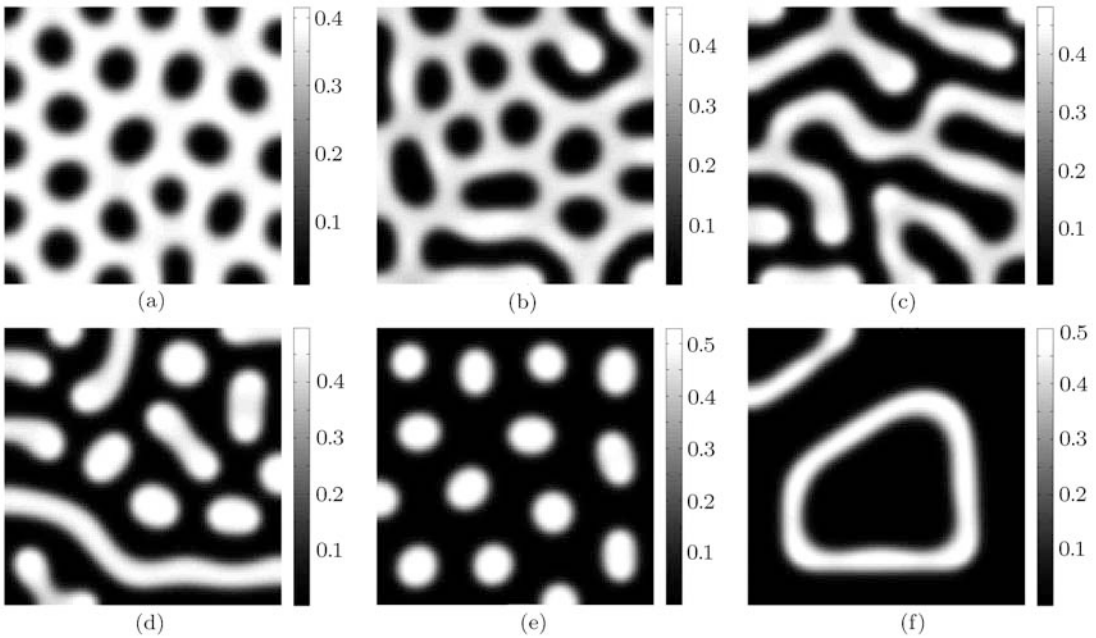


Fig. 4. Categories of Turing patterns of N in model (4) with parameters $\beta = 0.25, \gamma = 0.50, d_{11} = 0.0125$, $d_{12} = -0.005, d_{21} = 0.001, d_{22} = 1.0$. (a) $\mu = 0.0045296348$ ($\alpha = 0.708$); (b) $\mu = 0.0410864561$ ($\alpha = 0.682$); (c) $\mu = 0.0860794670$ ($\alpha = 0.65$); (d) $\mu = 0.1282604146$ ($\alpha = 0.62$); (e) $\mu = 0.2758937315$ ($\alpha = 0.515$); (f) $\mu = 0.2934691263$ ($\alpha = 0.5025$). Time: (a) 10000; (b)(c)(d) 2500; (e) 10000; (f) 4500.

4. Conclusions and remarks

In this paper, we present a multi-scale analysis for the Turing patterns formed in a predator–prey model with self-diffusion and cross-diffusion. We derive amplitude equations for the excited modes. From the amplitude equations (c.f., Eq. (13)) and the formulae of solutions (c.f., Eqs. (18) and (20)), we determine the relative stability of hexagons and stripe patterns near the onset of the Turing instability. From the amplitude equations, the stabilities of patterns to uniform and inhomogenous perturbations are determined separately.

We establish the amplitude equations by using the standard multiple-scale analysis, in which the control parameter α and the derivatives are expanded in terms of a small parameter ε and Fredholm alternative is used at each order of ε. For obtaining each order of ε, we use a series of transformations to convert Eq. (1) to Eq. (3). This is the very point where we can calculate the coefficients, such as τ_0, h, g_1, g_2.

In the predator–prey model (3) or (4), with the fixed parameters $\beta = 0.25$ and $\gamma = 0.5$, for obtaining the positive equilibrium, from condition (7), we know $\alpha > 0.5$, in which the corresponding $\mu_m = 0.2969842053$. That is to say, for model (4), the normalized distance to onset must satisfy $\mu < 0.2969842053 = \mu_m$. Furthermore, from Eqs. (16) and (17), we know that with the fixed parameter set (11), when $\alpha > 0.7112215740$ ($\alpha = 0.7112215740$ corresponds to $\mu_2 = 0$), the steady state (O) is the only stable solution of model (4). Therefore, $0 < \mu < 0.2969842053$ (i.e., $0.5 < \alpha < 0.7112215740$), which exhibits the emergency of Turing patterns. This is the reason why we select points '1' ($\alpha = 0.71$)—'6' ($\alpha = 0.505$) (c.f., Fig. 1).

In the numerical simulations, we adopt six 'points' in the line $\gamma = 0.5$ (c.f., Fig. 1). We have performed a large number of simulations and found that the model dynamics only exhibits these six typical patterns as shown in Fig. 4.

The methods and the results in the present paper can be applied to the pattern formation in the diffusive predator–prey model or other reaction–diffusion systems.

References

[1] Alonso D, Bartumeus F and Catalan J 2002 *Ecology* **83** 28

[2] Iida M, Mimura M and Ninomiya H 2006 *J. Math. Biol.* **53** 617

[3] Levin S 1992 *Ecology* **73** 1943

[4] Madzvamuse A and Maini P 2007 *J. Comp. Phys.* **225** 100

[5] McGehee E and Peacock-López E 2005 *Phys. Lett.* A **342** 90

[6] Morozov A and Petrovskii S 2009 *Bull. Math. Biol.* **71** 863

[7] Murray J 2003 *Mathematical Biology* (3rd Edition) (New York: Springer)

[8] Okubo A and Levin S 2001 *Diffusion and Ecological Problems: Modern Perspectives* (2nd Edition) (New York: Springer)

[9] Cantrell R and Cosner C 2003 *Spatial Ecology via Reaction-Diffusion Equations* (Chichester, UK: Wiley)

[10] Hoyle R 2006 *Pattern Formation: An Introduction to Methods* (Cambridge: Cambridge University Press)

[11] Wang W, Liu Q and Jin Z 2007 *Phys. Rev.* E **75** 051913

[12] Sun G, Jin Z, Liu Q and Li L 2008 *Chin. Phys. Lett.* **25** 2296

[13] Li L, Jin Z and Sun G 2008 *Chin. Phys. Lett.* **25** 3500

[14] Baurmann M, Gross T and Feudel U 2007 *J Theor. Biol.* **245** 220

[15] Bartumeus F, Alonso D and Catalan J 2001 *Phys.* A **295** 53

[16] Bjørnstad O N, Ims R A and Lambin X 1999 *TREE* **14** 427

[17] de Roos A M, McCauley E and Wilson W 1998 *Theor. Popu. Biol.* **53** 108

[18] Kawasaki K and Teramoto E 1979 *J. Math. Biol.* **8** 33

[19] Levin S and Segel L 1985 *SIAM Rev.* **27** 45

[20] Molofsky J 1994 *Ecology* **75** 30

[21] Neubert M, Kot M and Lewis M 1995 *Theor. Popu. Biol.* **48** 7

[22] Wang W, Zhang L, Wang H and Li Z 2010 *Ecol. Model* **221** 131

[23] Biktashev V, Brindley J, Holden A and Tsyganov M 2004 *Chaos* **14** 988

[24] Shukla J and Verma S 1981 *Bull. Math. Biol.* **43** 593

[25] Kerner E 1959 *Bull. Math. Biol.* **21** 217

[26] Shigesada N, Kawasaki K and Teramoto E 1979 *J. Theor. Biol.* **79** 83

[27] Chattopadhyay J and Tapaswi P 1997 *Acta Appl. Math.* **48** 1

[28] Chen L and Jüngel A 2006 *J. Differential Equations* **224** 39

[29] Dubey B, Das B and Hussain J 2001 *Ecol. Model* **141** 67

[30] Ko W and Ryu K 2008 *J. Math. Anal. Appl.* **341** 1133

[31] Ko W and Ryu K 2008 *Appl. Math. Lett.* **21** 1177

[32] Kuto K and Yamada Y 2004 *J. Differential Equations* **197** 315

[33] Pang R and Wang M 2004 *J. Differential Equations* **200** 245

[34] Pao C 2005 *Nonl. Anal.* **60** 1197

[35] Sun G, Jin Z, Liu Q and Li L 2008 *Chin. Phys.* B **17** 3936

[36] Vanag V and Epstein I 2009 *Phys. Chem. Chem. Phys.* **11** 897
[37] Dufiet V and Boissonade J 1992 *J. Chem. Phys.* **96** 664
[38] Dufiet V and Boissonade J 1992 *Phys.* A **188** 158
[39] Dufiet V and Boissonade J 1996 *Phys. Rev.* E **53** 4883
[40] Callahan T and Knobloch E 1999 *Phys.* D **132** 339
[41] Gunaratne G, Ouyang Q and Swinney H 1994 *Phys. Rev.* E **50** 2802
[42] Ipsen M, Hynne F and Sørensen P 1998 *Chaos* **8** 834
[43] Ipsen M, Hynne F and Sørensen P 2000 *Phys.* D **136** 66
[44] Newell A and Whitehead J 1969 *J. Fluid. Mech.* **38** 279
[45] Ouyang Q 2000 *Pattern Formation in Reaction-Diffusion Systems* (Shanghai: Shanghai Sci-Tech Education Publishing House)
[46] Ouyang Q, Gunaratne G and Swinney H 1993 *Chaos* **3** 707
[47] Peña B and Pérez-García C 2000 *Europhys. Lett.* **51** 300
[48] Peña B and Pérez-García C 2001 *Phys. Rev.* E **64** 56213
[49] Segel L 1969 *J. Fluid. Mech.* **38** 203
[50] Tang Y and Zhang W 2005 *J. Math. Biol.* **50** 699
[51] Berezovskaya F, Karev G and Arditi R 2001 *J. Math. Biol.* **43** 221
[52] Li B and Kuang Y 2007 *SIAM J. Appl. Math.* **67** 1453
[53] Yang L *Nonlinear Chemical Dynamics and Pattern Formation* http://hopf.chem.brandeis.edu/ yanglingfa/pattern/.
[54] Ciliberto S, Coullet P, Lega J, Pampaloni E and Perez-Garcia C 1990 *Phys. Rev. Lett.* **65** 2370